Time-dependent density functional theory calculations of near-edge X-ray absorption fine structure with short-range corrected functionals

Nicholas A. Besley,*[a] Michael J. G. Peach†[b] and David J. Tozer[b]

Received 29th June 2009, Accepted 10th September 2009
First published as an Advance Article on the web 25th September 2009
DOI: 10.1039/b912718f

We report calculations of core excitation energies and near-edge X-ray absorption fine structure (NEXAFS) spectra computed with time-dependent density functional theory (TDDFT). TDDFT with generalized gradient approximation and standard hybrid exchange–correlation functionals is known to underestimate core excitation energies. This failure is shown to be associated with the self-interaction error at short interelectronic distances. Short-range corrected hybrid functionals are shown to reduce the error in the computed core excitation energies for first and second row nuclei in a range of molecules to a level approaching that observed in more traditional excited states calculations in the ultraviolet region. NEXAFS spectra computed with the new functionals agree well with experiment and the pre-edge features in the NEXAFS spectra of plastocyanin are correctly predicted.

I. Introduction

Advances in modern synchrotron sources have provided spectroscopic techniques in the X-ray region with much greater sensitivity and resolution. This has increased the scope of these methods for use as analytical tools, and provided X-ray spectroscopy with a richness in structure that can match more traditional ultraviolet spectroscopy combined with the advantage that X-ray spectroscopy provides a local probe of structure. Currently, near edge X-ray absorption fine structure (NEXAFS) is used in a wide variety of fields, including materials science, surface science and biological chemistry.[1–4] In the future, it is likely that the application of these techniques will increase, fueling the demand for accurate calculations of core excited states.

A number of different theoretical approaches have been applied to study NEXAFS. Multiple scattering X_α methods,[5] static exchange (STEX)[6] and transition potential calculations[7] have been used to study a wide range of systems. More recently, there has been an effort to study the spectroscopy of core electrons within density functional theory (DFT). Accurate core excitation energies and core electron binding energies can be computed with a ΔKohn–Sham method,[8] wherein the excitation energy is simply the difference in energies from time-independent calculations on the ground and core excited states. Within this approach, some constraint, overlap criterion or intermediate optimization with a frozen core hole is used to prevent the collapse of the core hole during the self-consistent-field procedure for the excited state.[9–12] However, the calculation of NEXAFS spectra of large systems with a ΔKohn–Sham approach is problematic because of the very large number of core excited states, and hence separate DFT calculations, that are required.

Time-dependent density functional theory (TDDFT) in the adiabatic approximation provides a more efficient approach to computing NEXAFS spectra. Within TDDFT the core excited states can be computed by restricting the single excitation space to include only excitations from a subset of (core) orbitals[13–15] or using a resonant converged complex polarization propagator approach.[16,17] The main problem with TDDFT calculations of core excited states is that core excitation energies computed with standard exchange–correlation functionals are too low compared with experiment, and the extent of this underestimation increases with the nuclear charge of the atomic centers on which the core orbitals are localised. This error stems from the approximate exchange within the exchange–correlation functionals.[14,18–22] To correct for this error, exchange correlation functionals with increased fractions of Hartree–Fock (HF) exchange,[14,18,19] a combination of exchange–correlation functionals,[23] a self-interaction correction[20,21] and excited state methods that use exact exchange, such as CIS(D),[24] have been proposed.

There is an analogy between the calculation of core excited states and the calculation of charge transfer states. The failure of TDDFT to describe charge transfer states is well understood,[25] and the development of range separated hybrid exchange–correlation functionals has provided a solution to the charge transfer problem. In these functionals, the long range part of the exchange energy is usually evaluated primarily or completely using Hartree–Fock (HF) theory and DFT exchange is primarily used for the short range. In recent years, there has been considerable development and optimization of these functionals,[26–34] resulting in methods that provide accurate excitation energies for valence, Rydberg and charge transfer excited states.[28] However, long-range corrected functionals do not improve core excitation energies, and the predicted values remain too low.[22] This suggests that for core excited states, HF exchange is important in the short

[a] *School of Chemistry, University of Nottingham, University Park, Nottingham, UK NG7 2RD. E-mail: nick.besley@nottingham.ac.uk*
[b] *Department of Chemistry, University of Durham, South Road, Durham, UK DH1 3LE*
† Present address: Institut für Theoretische Physik, Freie Universität Berlin, Arnimallee 14, D-14195 Berlin, Germany

to mid range. The opposite splitting of the interelectronic repulsion operator, in which long range DFT is used in conjunction with short range HF, has been implemented.[35] This functional was called a screened hybrid functional and shows promise in the study of periodic systems.[36–38] Subsequently, a three range functional was introduced to combine the screened hybrid functional with a long-range corrected functional,[39,40] Recently, Hirao and coworkers optimized the LCgau-BOP method[31] for core excitations.[22] This functional introduces HF exchange at short range through the inclusion of a Gaussian function in the long-range corrected scheme. The resulting functional showed a substantial improvement in the predicted core-excitation energies when applied to first row nuclei.

The aim of the present study is to further investigate the characteristics of the range separation that are required for the accurate description of core excitations. The study is unashamedly semiempirical and pragmatic, but the findings are insightful and the resulting functionals are likely to be useful to those interested in computing core excitations.

II. Computational methods

Within the Tamm–Dancoff approximation (TDA)[41] of TDDFT, excitation energies and oscillator strengths are determined as the solutions to the eigenvalue equation[42]

$$\mathbf{AX} = \omega\mathbf{X} \tag{1}$$

The matrix **A** is given by

$$A_{ia\sigma,jb\tau} = \delta_{ij}\delta_{ab}\delta_{\sigma\tau}(\varepsilon_{a\sigma} - \varepsilon_{i\tau}) + (ia\sigma|jb\tau) + (ia\sigma|f_{\mathrm{XC}}|jb\tau) - K^{\mathrm{HF}}_{ia\sigma,jb\tau} \tag{2}$$

where

$$(ia\sigma|jb\tau) = \int\int \psi^*_{i\sigma}(\mathbf{r}_1)\psi^*_{a\sigma}(\mathbf{r}_1)\frac{1}{r_{12}}\psi_{j\tau}(\mathbf{r}_2)\psi_{b\tau}(\mathbf{r}_2)\,\mathrm{d}\mathbf{r}_1\mathrm{d}\mathbf{r}_2 \tag{3}$$

$$(ia\sigma|f_{\mathrm{XC}}|jb\tau) = \int \psi^*_{i\sigma}(\mathbf{r}_1)\psi_{a\sigma}(\mathbf{r}_1)\frac{\delta^2 E_{\mathrm{XC}}}{\delta\rho_\sigma(\mathbf{r}_1)\delta\rho_\tau(\mathbf{r}_2)} \times \psi_{j\tau}(\mathbf{r}_2)\psi^*_{b\tau}(\mathbf{r}_2)\,\mathrm{d}\mathbf{r}_1\mathrm{d}\mathbf{r}_2 \tag{4}$$

and ε_i are the orbital energies, E_{XC} is the exchange correlation functional and $K^{\mathrm{HF}}_{ia\sigma,jb\tau}$ is the HF exchange term. Within standard implementations of TDDFT, the calculation of core excited states becomes prohibitively expensive due to the large number of roots required to obtain the high energy core excited states. A practical solution to this problem is to restrict the single excitation space to include only excitations from the relevant core orbital(s).[13,15,43] This makes the calculation of core excited states of comparable expense to computing valence excited states whilst introducing a negligible error.[44] For small systems, the error can be evaluated directly by comparing the results from the calculations with the truncation of the excitation space to those from calculations with the full excitation space. For a range of core excitations from 1s orbitals, the largest error observed was 0.01 eV in the excitation energy and 0.011 in the oscillator strength.[44]

In standard long-range corrected functionals, the exchange–correlation functional can be expressed as

$$E^{\mathrm{LRC}}_{\mathrm{xc}} = E^{\mathrm{SR\text{-}DFT}}_{\mathrm{x}} + E^{\mathrm{LR\text{-}HF}}_{\mathrm{x}} + E^{\mathrm{DFT}}_{\mathrm{c}} \tag{5}$$

combining short-range DFT exchange with long-range HF exchange. These functionals have been further developed to include a small fraction of HF exchange at short range,[27,32] for example

$$E_{\mathrm{xc}} = c_{\mathrm{x}}E^{\mathrm{SR\text{-}HF}}_{\mathrm{x}} + E^{\mathrm{SR\text{-}DFT}}_{\mathrm{x}} + E^{\mathrm{LR\text{-}HF}}_{\mathrm{x}} + E^{\mathrm{DFT}}_{\mathrm{c}} \tag{6}$$

where c_{x} is a parameter that can be optimized. The most common approach to achieve the partitioning between long and short components is to split the electron repulsion operator in the evaluation of the exchange energy according to the error function

$$\frac{1}{r_{12}} \equiv \frac{\mathrm{erf}(\mu r_{12})}{r_{12}} + \frac{\mathrm{erfc}(\mu r_{12})}{r_{12}} \tag{7}$$

where $r_{12} = |\mathbf{r}_1 - \mathbf{r}_2|$ and erfc = 1 − erf.

In order to generate a flexible function with varying amounts of HF exchange in both the short and long range we consider the following partitioning of the electron repulsion operator

$$\frac{1}{r_{12}} \equiv C_{\mathrm{SHF}}\frac{\mathrm{erfc}(\mu_{\mathrm{SR}}r_{12})}{r_{12}} - C_{\mathrm{SHF}}\frac{\mathrm{erfc}(\mu_{\mathrm{SR}}r_{12})}{r_{12}} + C_{\mathrm{LHF}}\frac{\mathrm{erf}(\mu_{\mathrm{LR}}r_{12})}{r_{12}} - C_{\mathrm{LHF}}\frac{\mathrm{erf}(\mu_{\mathrm{LR}}r_{12})}{r_{12}} + \frac{1}{r_{12}} \tag{8}$$

Treating the first and third terms of eqn (8) with HF exchange and the remaining terms with DFT exchange leads to the following functional

$$E^{\mathrm{SRC\text{-}1}}_{\mathrm{xc}} = C_{\mathrm{SHF}}E^{\mathrm{SR\text{-}HF}}_{\mathrm{x}}(\mu_{\mathrm{SR}}) - C_{\mathrm{SHF}}E^{\mathrm{SR\text{-}DFT}}_{\mathrm{x}}(\mu_{\mathrm{SR}}) + C_{\mathrm{LHF}}E^{\mathrm{LR\text{-}HF}}_{\mathrm{x}}(\mu_{\mathrm{LR}}) - C_{\mathrm{LHF}}E^{\mathrm{LR\text{-}DFT}}_{\mathrm{x}}(\mu_{\mathrm{LR}}) + E^{\mathrm{DFT}}_{\mathrm{x}} + E^{\mathrm{DFT}}_{\mathrm{c}} \tag{9}$$

where

$$E^{\mathrm{LR\text{-}HF}}_{\mathrm{x}} = -\frac{1}{2}\sum_\sigma\sum_{i,j}^{\mathrm{occ}}\int\int \psi^*_{i\sigma}(\mathbf{r}_1)\psi^*_{j\sigma}(\mathbf{r}_1) \times \frac{\mathrm{erf}(\mu_{\mathrm{LR}}r_{12})}{r_{12}}\psi_{i\sigma}(\mathbf{r}_2)\psi_{j\sigma}(\mathbf{r}_2)\,\mathrm{d}\mathbf{r}_1\mathrm{d}\mathbf{r}_2 \tag{10}$$

and

$$E^{\mathrm{SR\text{-}HF}}_{\mathrm{x}} = -\frac{1}{2}\sum_\sigma\sum_{i,j}^{\mathrm{occ}}\int\int \psi^*_{i\sigma}(\mathbf{r}_1)\psi^*_{j\sigma}(\mathbf{r}_1) \times \frac{\mathrm{erfc}(\mu_{\mathrm{SR}}r_{12})}{r_{12}}\psi_{i\sigma}(\mathbf{r}_2)\psi_{j\sigma}(\mathbf{r}_2)\,\mathrm{d}\mathbf{r}_1\mathrm{d}\mathbf{r}_2 \tag{11}$$

respectively. The long and short range DFT exchange are computed from modifying the usual exchange energy[30]

$$E_{\mathrm{x}} = -\frac{1}{2}\sum_\sigma\int \rho_\sigma^{4/3}K_\sigma\,\mathrm{d}\mathbf{r} \tag{12}$$

to give

$$E_{\mathrm{x}}^{\mathrm{LR\text{-}DFT}} = -\frac{1}{2}\sum_{\sigma}\int \rho_{\sigma}^{4/3} K_{\sigma}\frac{8}{3}a_{\sigma} \times \left[\sqrt{\pi}\,\mathrm{erf}\left(\frac{1}{2a_{\sigma}^{\mathrm{LR}}}\right) + 2a_{\sigma}(b_{\sigma}-c_{\sigma})\right]\mathrm{d}\mathbf{r} \quad (13)$$

and

$$E_{\mathrm{x}}^{\mathrm{SR\text{-}DFT}} = -\frac{1}{2}\sum_{\sigma}\int \rho_{\sigma}^{4/3} K_{\sigma} \times \left\{1 - \frac{8}{3}a_{\sigma}\left[\sqrt{\pi}\,\mathrm{erf}\left(\frac{1}{2a_{\sigma}^{\mathrm{SR}}}\right) + 2a_{\sigma}(b_{\sigma}-c_{\sigma})\right]\right\}\mathrm{d}\mathbf{r} \quad (14)$$

where

$$a_{\sigma}^{\mathrm{SR}} = \frac{\mu_{\mathrm{SR}}}{6\sqrt{\pi}}\rho_{\sigma}^{-1/3}K_{\sigma}^{1/2} \quad (15)$$

$$a_{\sigma}^{\mathrm{LR}} = \frac{\mu_{\mathrm{LR}}}{6\sqrt{\pi}}\rho_{\sigma}^{-1/3}K_{\sigma}^{1/2} \quad (16)$$

$$b_{\sigma} = \exp\left(-\frac{1}{4a_{\sigma}^{2}}\right) - 1 \quad (17)$$

and

$$c_{\sigma} = 2a_{\sigma}^{2}b_{\sigma} + \tfrac{1}{2} \quad (18)$$

If $C_{\mathrm{LHF}} = 0$, the functional yields a short-range corrected analogue of eqn (5). For this functional the fraction of HF exchange will be C_{SHF} at $r_{12} = 0$, and fall to zero as r_{12} increases. This functional has two parameters, C_{SHF} and the attenuation parameter μ_{SR}, to be optimized. If $C_{\mathrm{LHF}} \neq 0$ the fraction of HF exchange approaches C_{LHF} at long range. This form of the functional has four parameters, C_{SHF}, C_{LHF}, μ_{SR} and μ_{LR}, to be optimized. If $\mu_{\mathrm{LR}} = \mu_{\mathrm{SR}}$ then the functional form is equivalent to the CAM-B3LYP functional of Yanai *et al.*,[27] which has the following partition

$$\frac{1}{r_{12}} \equiv \frac{1-[\alpha+\beta\,\mathrm{erf}(\mu r_{12})]}{r_{12}} + \frac{\alpha+\beta\,\mathrm{erf}(\mu r_{12})}{r_{12}} \quad (19)$$

and the two functionals can be related *via*

$$\alpha = C_{\mathrm{SHF}} \quad (20)$$

$$\beta = C_{\mathrm{LHF}} - C_{\mathrm{SHF}} \quad (21)$$

which results in β being negative for a short-range corrected functional. A further closely related form of a short-range corrected functional is also considered

$$E_{\mathrm{xc}}^{\mathrm{SRC\text{-}2}} = C_{\mathrm{SHF}}E_{\mathrm{x}}^{\mathrm{SR\text{-}HF}}(\mu_{\mathrm{SR}}) + (1-C_{\mathrm{SHF}})E_{\mathrm{x}}^{\mathrm{SR\text{-}DFT}}(\mu_{\mathrm{SR}}) + C_{\mathrm{LHF}}E_{\mathrm{x}}^{\mathrm{LR\text{-}HF}}(\mu_{\mathrm{LR}}) + (1-C_{\mathrm{LHF}})E_{\mathrm{x}}^{\mathrm{LR\text{-}DFT}}(\mu_{\mathrm{LR}}) + E_{\mathrm{c}}^{\mathrm{DFT}} \quad (22)$$

When $\mu_{\mathrm{SR}} = \mu_{\mathrm{LR}}$, this functional is equivalent to the SRC-1 functional (eqn (9)). However, if $\mu_{\mathrm{SR}} \neq \mu_{\mathrm{LR}}$, the two functionals differ, and the SRC-2 functional no longer corresponds to a rigorous partitioning of the electron-repulsion operator (eqn (8)).

In this work, the exchange functional of Becke was used[45] for treating the DFT contribution to the exchange energy. For the correlation functional the following combination of LYP[46] and VWN[47] functionals was used.

$$E_{\mathrm{c}} = 0.81\mathrm{LYP} + 0.19\mathrm{VWN} \quad (23)$$

This combination of correlation functionals gives slightly better results than the LYP functional on its own, and the remaining parameters are determined by minimizing the mean absolute error of the computed core excitation energies with experimental data.

Standard hybrid functionals, such as B3LYP, are known to provide poor core excitation energies, and are not a good benchmark to demonstrate the improved performance of new exchange–correlation functionals. One option is to use the BHHLYP functional, which has 50% HF exchange. However, while this functional represents a significant improvement over B3LYP, its performance remains relatively poor. In this work, to show the effectiveness of the short-range corrected functionals described, they are compared with a modified version of the B3LYP functional in which the constant proportion of HF exchange is optimized[14] to give the best agreement with the experimental core excitation energies.

All calculations were done using the ground state structure optimized at the MP2/cc-pVTZ level. The integration grid was the 100 point Euler–Maclaurin radial grid and the 302 point Lebedev angular grid. Relativistic effects provide an additional complication with the computation of core excited states, leading to a significant lowering of the energy of core orbitals for heavier elements. The effect of relativity was estimated from the lowering of the core orbital energy between non-relativistic and relativistic HF/cc-pCVTZ calculations. This lowering in energy is insensitive to the molecular environment of the core orbital, and the corrections used in this work were derived from atomic calculations since this avoids the need for relativistic calculations on large systems. The relativistic energy was computed with the Douglas–Kroll–Hess Hamiltonian[48] with the MOLPRO software package.[49] The calculated corrections to the excitation energies are 3.4 eV, 4.6 eV, 5.9 eV, 7.9 eV and 79.7 eV for Si, P, S, Cl and Cu, respectively. Corresponding corrections for the first row elements are much smaller, and have not been included. In this work, all core excitations from second row nuclei have been corrected for relativity. The 6-311(2+,2+)G** basis set was used for all core excitation calculations, and the calculations were performed with a development version of Q-Chem.[50]

III. Results and discussion

Before discussing short-range corrected functionals, it is informative to examine the use of a long-range corrected functional for core excitations. Table 1 shows the calculated excitation energies for a representative subset of the core excited states studied in this work with the standard BLYP functional and its long-range corrected analogue [eqn (5)] with a standard value of $\mu = 0.4a_0^{-1}$. The excitation energies predicted with BLYP show the well documented large underestimation of the values from experiment. Also shown

Table 1 Predicted core excitation energies (in eV) with BLYP and LRC-BLYP functionals together with the Λ diagnostic

Excitation	Exp.	BLYP	Λ	LRC-BLYP
CO C(1s) → π*	287.4	271.1	0.18	270.9
CO C(1s) → 3s	292.4	272.7	0.04	274.9
CO O(1s) → π*	534.2	512.0	0.14	512.3
CO O(1s) → 3s	538.9	513.6	0.03	515.3
HF F(1s) → σ*	687.4	659.7	0.08	660.6
SiH_4 Si(1s) → σ*	1842.5	1784.1	0.03	1785.3
H_2S S(1s) → σ*	2473.1	2402.3	0.04	2403.3
H_2S S(1s) → 4p	2476.3	2403.5	0.01	2406.0
HCl Cl(1s) → σ*	2823.9	2749.8	0.02	2749.7
HCl Cl(1s) → $4p_\pi$	2827.8	2750.3	0.01	2752.7

in Table 1 are calculated BLYP values of the Λ diagnostic of Peach *et al.*[51] The values of Λ are low, consistent with the failure of the generalized gradient approximation functional. Applying the long-range corrected BLYP functional has a small effect on the core excitations to Rydberg orbitals, but does not correct for the large underestimation of the core-excitation energies relative to experiment. This illustrates that the description of the exchange in the long range is not the critical factor in the failure of TDDFT for core excited states.

Tables 2 and 3 show predicted core excitation energies to valence and Rydberg states for a number of first row nuclei with hybrid and short-range corrected functionals. Core excitation energies with the hybrid B3LYP functional are too low, indicating that 20% HF exchange is not sufficient. Overall, B3LYP has a mean absolute deviation (MAD) with experiment of 12.7 eV and 12.9 eV for the valence and Rydberg states, respectively. Previous studies have also shown that a significantly higher proportion of HF is required.[14,18,19] Optimizing the proportion of HF exchange in the B3LYP functional on both valence and Rydberg states, yields a value of 58% HF exchange, with a correspondingly reduced proportion of B88 exchange of 39% and 8% Slater exchange. This functional is denoted $BH^{0.58}LYP$. This functional reduces the error in the excitation energies to 0.7 eV and 0.9 eV for the valence and Rydberg states, respectively. These results better represent the level accuracy that a hybrid functional with a fixed fraction of HF exchange can achieve, and provide benchmark values that can be used to assess any range-corrected functional.

For the short-range corrected functional with no HF exchange at long range, *i.e.* $C_{LHF} = 0$, optimization of the parameters for excitations to valence and Rydberg states gives $C_{SHF} = 0.57$ and $\mu_{SHF} = 0.30a_0^{-1}$. The variation of the fraction of HF exchange with r_{12} is shown in Fig. 1, and is 57% at $r_{12} = 0$ and falls off slowly as r_{12} increases. For the core → valence states the MAD is 0.6 eV, which is marginally better than for the $BH^{0.58}LYP$ functional. For the core → Rydberg states there is a larger improvement over $BH^{0.58}LYP$, and the MAD is reduced to 0.5 eV. The largest error is 1.9 eV for the C(1s) → π* excitation in CO.

We now consider introducing HF exchange at long-range. For the SRC-1 functional form, optimization of the parameters gives $C_{SHF} = 0.50$, $\mu_{SR} = 0.56a_0^{-1}$, $C_{LHF} = 0.17$ and $\mu_{LR} = 2.45a_0^{-1}$. The resulting functional shows an improved performance, with a reduction in the MADs for core → valence and core → Rydberg excitations to 0.5 eV and 0.4 eV, respectively. The largest error arises for the C(1s) → π* excitation in CO. For the SRC-2 functional form the following parameters are obtained, $C_{SHF} = 0.55$, $\mu_{SR} = 0.69a_0^{-1}$, $C_{LHF} = 0.08$ and $\mu_{LR} = 1.02a_0^{-1}$. This form of the functional shows a significant improvement in accuracy of the core → valence states excitations, with the MAD reduced to 0.3 eV and the largest error 0.8 eV for the C(1s) → 3s excitation in ethene. The level of accuracy of these functionals is approaching that which is achieved for traditional valence electron excitations, and is significantly more accurate than previously reported methods for computing core excitations from first row nuclei.[8,18,22,24] For a similar set of molecules, MADs of 0.6 eV, 0.8 eV and 1.2 eV were obtained with TDDFT with the core-valence-Rydberg B3LYP and LCgau-core-BOP functionals, and a modified CIS(D) method, respectively.

The variation of the fraction of HF exchange with r_{12} (Fig. 1) provides some insight into the origin of this improvement. All the functionals have a fraction of HF exchange at $r_{12} = 0$ of 0.5 to 0.6. For the SRC-1 functional, the fraction of HF exchange in the mid-range is similar to the functional with $C_{LHF} = 0$. However, at short-range the behaviour is different.

Table 2 Computed excitation energies (in eV) for core → valence transitions for first row nuclei. Deviations from experiment shown in parenthesis. Experimental data from ref. 56–65

Excitation	Exp.	B3LYP	$BH^{0.58}LYP$	SRC1-BLYP $C_{SHF} = 0.57$, $\mu_{SR} = 0.30a_0^{-1}$, $C_{LHF} = 0.00$	SRC1-BLYP $C_{SHF} = 0.50$, $\mu_{SR} = 0.56a_0^{-1}$, $C_{LHF} = 0.17$, $\mu_{LR} = 2.45a_0^{-1}$	SRC2-BLYP $C_{SHF} = 0.55$, $\mu_{SR} = 0.69a_0^{-1}$, $C_{LHF} = 0.08$, $\mu_{LR} = 1.02a_0^{-1}$
C_2H_4 C(1s) → π*	284.7	274.2 (−10.5)	284.7 (0.0)	284.6 (+0.1)	285.1 (+0.4)	285.3 (+0.6)
C_2H_2 C(1s) → π*	285.8	275.2 (−10.6)	285.8 (0.0)	285.7 (−0.1)	286.1 (+0.3)	286.3 (+0.5)
H_2CO C(1s) → π*	286.0	275.1 (−10.9)	284.9 (−1.1)	285.0 (−1.0)	285.5 (−0.5)	286.0 (0.0)
CO C(1s) → π*	287.4	276.1 (−11.3)	285.5 (−2.0)	285.5 (−1.9)	286.1 (−1.3)	286.7 (+0.7)
CO_2 C(1s) → π*	290.8	279.6 (−11.2)	289.3 (−1.5)	289.3 (−1.5)	289.8 (−1.0)	290.4 (−0.4)
N_2 N(1s) → π*	401.0	388.4 (−12.6)	400.3 (−0.7)	400.2 (−0.8)	400.6 (−0.4)	400.7 (−0.3)
H_2CO O(1s) → π*	530.8	516.5 (−14.3)	531.1 (+0.3)	530.8 (0.0)	530.8 (0.0)	530.8 (0.0)
CO O(1s) → π*	534.2	519.6 (−14.6)	534.7 (+0.5)	534.4 (+0.2)	534.4 (+0.2)	534.2 (0.0)
HF F(1s) → σ*	687.4	669.3 (−18.1)	687.4 (0.0)	687.2 (−0.2)	686.7 (−0.7)	686.9 (−0.5)
MAD[a]	—	12.7	0.7	0.6	0.5	0.3

[a] Mean absolute deviation.

Table 3 Computed excitation energies (in eV) for core → Rydberg transitions for first row nuclei. Deviations from experiment shown in parenthesis. Experimental data from ref. 56,57,59–65

Excitation	Exp.	B3LYP	$BH^{0.58}LYP$	SRC1-BLYP $C_{SHF} = 0.57$, $\mu_{SR} = 0.30a_0^{-1}$, $C_{LHF} = 0.00$	SRC1-BLYP $C_{SHF} = 0.50$, $\mu_{SR} = 0.56a_0^{-1}$, $C_{LHF} = 0.17$, $\mu_{LR} = 2.45a_0^{-1}$	SRC2-BLYP $C_{SHF} = 0.55$, $\mu_{SR} = 0.69a_0^{-1}$, $C_{LHF} = 0.08$, $\mu_{LR} = 1.02a_0^{-1}$
C_2H_4 C(1s) → 3s	287.1	275.7 (−11.4)	288.3 (+1.2)	287.7 (+0.6)	287.8 (+0.7)	287.9 (+0.8)
C_2H_2 C(1s) → 3s	287.7	276.1 (−11.6)	288.7 (+1.0)	288.1 (+0.4)	288.3 (+0.6)	288.3 (+0.6)
C_2H_2 C(1s) → $3p_\pi$	288.7	276.9 (−11.8)	290.1 (+1.4)	288.5 (−0.2)	289.3 (+0.6)	288.6 (−0.1)
C_2H_2 C(1s) → $3p_\sigma$	288.8	276.5 (−12.3)	289.5 (+0.7)	289.1 (+0.3)	288.8 (0.0)	289.2 (+0.4)
H_2CO C(1s) → $3sa_1$	290.2	278.3 (−11.9)	290.7 (+0.5)	290.2 (0.0)	290.3 (+0.1)	290.7 (+0.5)
H_2CO C(1s) → $3pb_2$	291.3	279.4 (−11.9)	291.5 (+0.2)	290.9 (−0.4)	291.1 (−0.2)	291.4 (+0.1)
H_2CO C(1s) → $3pa_1$	291.7	279.1 (−12.6)	292.5 (+0.8)	291.6 (−0.1)	291.7 (0.0)	291.9 (+0.2)
CO C(1s) → 3s	292.4	279.4 (−13.0)	292.4 (0.0)	291.6 (−0.8)	291.7 (−0.7)	292.0 (−0.4)
CO C(1s) → $3p_\pi$	293.3	280.1 (−13.2)	293.3 (0.0)	292.3 (−1.0)	292.4 (−0.9)	292.6 (−0.7)
CO C(1s) → $3p_\sigma$	293.5	280.0 (−13.5)	293.4 (−0.1)	292.3 (−1.2)	292.4 (−1.1)	292.6 (−0.9)
CO_2 C(1s) → 3s	292.7	280.0 (−12.7)	292.5 (−0.2)	292.2 (−0.5)	292.5 (−0.2)	292.9 (+0.2)
CO_2 C(1s) → $3p_\pi$	295.0	281.9 (−13.1)	295.7 (+0.7)	294.5 (−0.5)	294.6 (−0.4)	294.9 (−0.1)
N_2 N(1s) → 3s	406.2	391.8 (−14.4)	407.1 (+0.9)	406.4 (+0.2)	406.4 (−0.2)	406.4 (−0.2)
N_2 N(1s) → $3p_\pi$	407.1	392.5 (−14.6)	408.2 (+1.1)	407.2 (+0.1)	407.2 (+0.1)	407.1 (0.0)
N_2 N(1s) → $3p_\sigma$	407.3	392.5 (−14.8)	408.4 (+1.1)	407.2 (−0.1)	407.2 (−0.1)	407.2 (−0.1)
H_2CO O(1s) → $3sa_1$	535.4	519.9 (−15.5)	537.9 (+2.5)	536.8 (+1.4)	535.7 (−0.8)	536.1 (+0.7)
H_2CO O(1s) → $3pa_1$	536.3	520.7 (−15.6)	538.5 (+2.2)	537.4 (+1.1)	537.3 (+1.0)	536.9 (+0.6)
CO O(1s) → 3s	538.9	522.6 (−16.3)	540.1 (+1.2)	539.4 (+0.5)	539.2 (+0.3)	539.0 (+0.1)
CO O(1s) → 3pπ	539.9	523.3 (−16.6)	541.3 (+1.4)	540.2 (+0.3)	540.0 (+0.1)	539.7 (+0.2)
MAD[a]	—	12.9	0.9	0.5	0.4	0.4

[a] Mean absolute deviation.

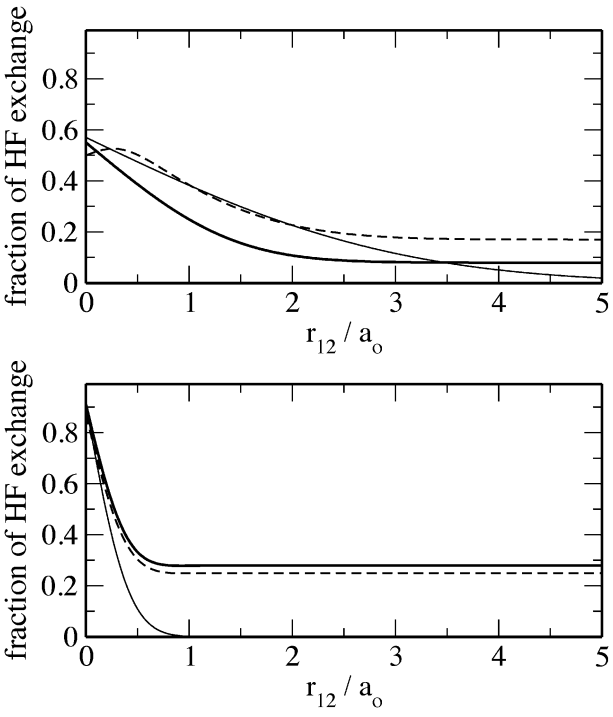

Fig. 1 Variation of the fraction of Hartree–Fock exchange. Top panel: narrow line—$C_{SHF} = 0.57$, $\mu_{SR} = 0.30a_0^{-1}$ and $C_{LHF} = 0.00$; broken line—SRC-1 functional with $C_{SHF} = 0.50$, $\mu_{SR} = 0.56a_0^{-1}$, $C_{LHF} = 0.17$ and $\mu_{LR} = 2.45a_0^{-1}$; bold line—SRC-2 functional with $C_{SHF} = 0.55$, $\mu_{SR} = 0.69a_0^{-1}$, $C_{LHF} = 0.08$ and $\mu_{LR} = 1.02a_0^{-1}$. Lower panel: narrow line—$C_{SHF} = 0.85$, $\mu_{SR} = 1.68a_0^{-1}$ and $C_{LHF} = 0.00$; broken line—SRC-1 functional with $C_{SHF} = 0.87$, $\mu_{SR} = 2.20a_0^{-1}$, $C_{LHF} = 0.25$ and $\mu_{LR} = 1.80a_0^{-1}$; bold line—SRC-2 functional with $C_{SHF} = 0.91$, $\mu_{SR} = 2.20a_0^{-1}$, $C_{LHF} = 0.28$ and $\mu_{LR} = 1.80a_0^{-1}$.

At short range with $C_{LHF} \neq 0$, the fraction of HF exchange rises before falling. This comes from the long-range HF component, which has a large value for μ_{LR}. The SRC-2 functional provides the most accurate excitation energies for the first row nuclei, in particular there is a reduction in the MAD for the core → valence excitations. For this functional, the HF exchange component at short-range falls more rapidly and only extends to short r_{12}. This reduces the fraction of HF in the mid-range while retaining a greater proportion of HF exchange at long range. For this functional, there is no initial rise in the fraction of HF exchange at short-range, as observed with the SRC-1 functional form. As discussed in the Computational methods, this functional form does not conform to a rigorous partitioning of the electron repulsion operator. For this functional form, the electron repulsion operator is partitioned

$$\frac{1}{r_{12}} \equiv C_{SHF}\frac{\mathrm{erfc}(\mu_{SR}r_{12})}{r_{12}} - C_{SHF}\frac{\mathrm{erfc}(\mu_{SR}r_{12})}{r_{12}} + \frac{\mathrm{erfc}(\mu_{SR}r_{12})}{r_{12}} + C_{LHF}\frac{\mathrm{erf}(\mu_{LR}r_{12})}{r_{12}} - C_{LHF}\frac{\mathrm{erf}(\mu_{LR}r_{12})}{r_{12}} + \frac{\mathrm{erf}(\mu_{LR}r_{12})}{r_{12}} \quad (24)$$

which is not valid when $\mu_{SR} \neq \mu_{LR}$. The deviation from this identity is illustrated in Fig. 2, which shows the variation of $\mathrm{erfc}(\mu_{SR}r_{12}) + \mathrm{erf}(\mu_{LR}r_{12})$ with r_{12} for the optimized SRC-2 functional. The deviation from the identity condition occurs at short-range where $\mathrm{erfc}(\mu_{SR}r_{12}) + \mathrm{erf}(\mu_{LR}r_{12}) \geq 1$. Consequently, there is effectively more exchange at short range, and this is consistent with the absence of the initial rise in the fraction of HF exchange for the SRC-2 form.

Recent work by Chai and Head-Gordon identified a conserved region in the mid-range for long-range corrected

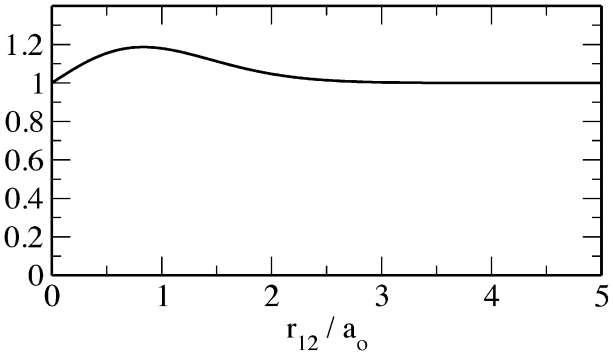

Fig. 2 Graph of $\mathrm{erfc}(\mu_{SR}r_{12}) + \mathrm{erf}(\mu_{LR}r_{12})$, $\mu_{SR} = 0.69a_0^{-1}$ and $\mu_{LR} = 1.02a_0^{-1}$.

functionals.[33] These functionals were shown to have about 30% HF exchange at $0.8a_0$. It is interesting to note that Fig. 1 shows that the optimized SRC-2 functional is also consistent with this condition, and is much closer to this point than the functional with $C_{LHF} = 0$. However, it should be emphasized that these functionals have been designed for computing core excitations and are unlikely to be competitive with the best functionals for thermodynamic properties. It is known that at long-range the correct proportion of HF exchange is 1. The optimized values of C_{LHF} for the short-range functionals differ significantly from this. The reason for this is that the functional form does not have sufficient flexibility to fall from a high value at $r_{12} = 0$ and then rise to unity in a sufficiently narrow range of r_{12} and for core excitations the required behaviour at short-range is dominant.

Now we consider core excitations from second row nuclei in Table 4. B3LYP gives a MAD from experiment of over 50 eV. The increase in error for B3LYP is a consequence of the increased nuclear charge. Varying the constant fraction of HF exchange in the hybrid functional gives a value of 71% with an associated MAD of 1.1 eV. This is consistent with previous work which has shown that higher proportions of HF are required for core excitations from second row nuclei.[19]

For the short-range corrected functional, the parameters obtained for the first row nuclei are not appropriate for the second row nuclei, and the functionals need to be reoptimized. Optimization of the short-range corrected functional with $C_{LHF} = 0$ gives $C_{SHF} = 0.85$, $\mu_{SR} = 1.68a_0^{-1}$. For this functional the MAD is reduced to 0.6 eV and the largest error is 2.0 eV. Including HF exchange at long range gives $C_{SHF} = 0.87$, $\mu_{SR} = 2.20a_0^{-1}$, $C_{LHF} = 0.25$ and $\mu_{LR} = 1.80a_0^{-1}$ for the SRC-1 functional and $C_{SHF} = 0.91$, $\mu_{SR} = 2.20a_0^{-1}$, $C_{LHF} = 0.28$ and $\mu_{LR} = 1.80a_0^{-1}$ for SRC-2. For both functionals the MAD reduces to 0.4 eV and the largest error is reduced to 0.9 and 1.0 eV. This slightly larger error compared to the first row nuclei may be associated with the treatment of relativistic effects. For the second row nuclei the magnitude of these effects are significant, and the calculations are likely to benefit from relativistic corrections being incorporated directly into the TDDFT calculations. The variation of the amount of HF exchange with r_{12} is shown in Fig. 1. At short range, all the functionals have similar behaviour. The functionals have a high proportion of HF exchange at $r_{12} = 0$, which falls rapidly as r_{12} increases due to the large μ_{SR} values. This more rapid fall in the fraction of HF exchange at short-range for second row nuclei is a reflection of the more compact 1s orbitals for heavier nuclei. The functionals begin to differ at around $r_{12} = 0.8$, with the functionals with long range HF leveling off. These functionals provide a high level of accuracy that is comparable to that achieved for the first row nuclei and confirms that introducing HF exchange at short range does correct core excitations computed with TDDFT.

The first term in matrix **A** in eqn (2) is the orbital energy difference which will be dominant for core excitations, and it is informative to consider how these energies are affected by the short and long-range corrections. Fig. 3 shows the change in orbital energies for valence, Rydberg and core orbitals in CO and HCl for short-range and long-range corrected functionals compared BLYP. The long-range corrected functional has $\mu = 0.3a_0^{-1}$ and the short-range corrected functional has the SRC-1 form with $C_{LHF} = 0$ and the appropriate parameters for first and second row nuclei. The effect of the long-range correction is to increase the unoccupied Rydberg and valence orbital energies slightly. There is also a decrease in

Table 4 Computed excitation energies (in eV) for second row nuclei. Deviations from experiment shown in parenthesis. Experimental data from ref. 66–71

Excitation	Exp.	B3LYP	$BH^{0.71}LYP$	SRC1-BLYP $C_{SHF} = 0.85$, $\mu_{SR} = 1.68a_0^{-1}$, $C_{LHF} = 0.00$	SRC1-BLYP $C_{SHF} = 0.87$, $\mu_{SR} = 2.20a_0^{-1}$, $C_{LHF} = 0.25$, $\mu_{LR} = 1.80a_0^{-1}$	SRC2-BLYP $C_{SHF} = 0.91$, $\mu_{SR} = 2.20a_0^{-1}$, $C_{LHF} = 0.28$, $\mu_{LR} = 1.80a_0^{-1}$
SiH_4 Si(1s) $\rightarrow \sigma^*$	1842.5	1800.9 (−41.6)	1845.0 (+2.5)	1842.7 (+0.2)	1843.1 (+0.6)	1842.5 (0.0)
PH_3 P(1s) $\rightarrow \sigma^*$	2145.8	2099.6 (−46.2)	2147.6 (+0.8)	2146.1 (+0.3)	2146.2 (+0.4)	2145.8 (0.0)
H_2S S(1s) $\rightarrow \sigma^*$	2473.1	2421.8 (−51.3)	2472.1 (−1.0)	2473.1 (0.0)	2473.1 (0.0)	2472.9 (−0.2)
H_2S S(1s) $\rightarrow$ 4p	2476.3	2423.5 (−52.8)	2476.8 (+0.5)	2474.3 (−2.0)	2467.4 (−0.9)	2475.3 (−1.0)
SO_2 S(1s) $\rightarrow \pi^*$	2473.8	2422.4 (−51.4)	2471.9 (−1.9)	2473.6 (−0.2)	2473.4 (−0.4)	2473.1 (−0.7)
SO_2 S(1s) $\rightarrow$ 4p	2478.4	2427.8 (−50.6)	2478.8 (+0.4)	2478.7 (+0.3)	2478.5 (+0.1)	2479.0 (+0.6)
HCl Cl(1s) $\rightarrow \sigma^*$	2823.9	2769.1 (−54.8)	2822.7 (−1.2)	2824.4 (+0.5)	2824.6 (+0.7)	2824.5 (+0.6)
HCl Cl(1s) $\rightarrow 4p_\pi$	2827.8	2771.4 (−56.4)	2827.6 (−0.2)	2826.5 (−1.3)	2827.5 (−0.3)	2827.5 (−0.3)
Cl_2 Cl(1s) $\rightarrow \sigma_u^*$	2821.3	2764.7 (−54.6)	2819.3 (−2.0)	2822.0 (+0.7)	2821.8 (+0.5)	2821.7 (+0.4)
Cl_2 Cl(1s) $\rightarrow$ 4p	2828.5	2770.7 (−55.8)	2829.1 (+0.6)	2827.7 (−0.8)	2828.8 (+0.5)	2828.8 (+0.3)
MAD[a]	—	51.6	1.1	0.6	0.4	0.4

[a] Mean absolute deviation.

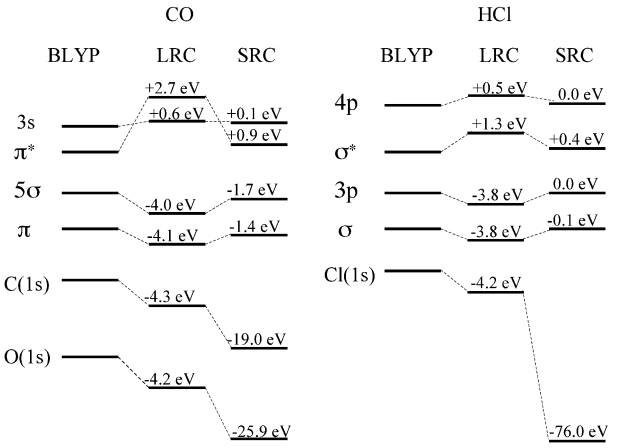

Fig. 3 Change in the orbitals energies between BLYP and long-range and short-range corrected (SRC-1) analogues.

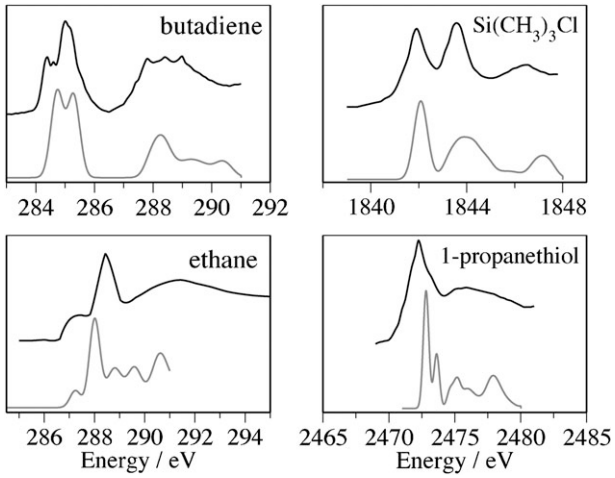

Fig. 4 Experimental spectra (upper line) and computed spectra (lower line). Experimental spectra adapted from ref. 52, 72, 73.

the energies of the occupied valence and core orbitals by about 4 eV. Of particular relevance for the calculation of core excitation energies is that the magnitude of the energy change of the core orbitals is much smaller than the errors in the computed core excitation energies and there is no significant difference between the energy changes of the different core orbitals. Similarly, asymptotically correcting the potential would have little effect on the core orbitals and would just lead to an increase in the Rydberg orbital energies. By contrast, the short-range corrected functional has a very significant effect on the core orbital energies which increases with the nuclear charge of the relevant nuclei, and has little effect on the valence orbital energies. Furthermore, the amount the core orbital is lowered in energy is comparable to the underestimation of the core excitation energy (see Table 1). These observations, which are to be expected based on the exact exchange operator in the orbital equations, are fully consistent with the results in Tables 2–4, providing some insight into the different behaviour of short and long-range corrections. Although the orbital energy difference is dominant in eqn (2), the remaining terms cannot be neglected. For core excitations from the second row elements, there remains a significant difference between the orbital energy difference and the computed TDDFT excitation energy. For the Cl(1s) $\rightarrow$ σ* excitation in HCl the orbital energy difference is over 3 eV greater than the computed excitation energy.

Fig. 4 shows experimental and computed NEXAFS spectra for four molecules not included in the parameterization of the functionals. The computed spectra have been generated by representing each excitation by a Gaussian function with a full-width at half maximum of 0.3 eV. Carbon K-edge spectra are shown for butadiene and ethane. The computed spectra is evaluated with the SRC-1 functional, which was optimized for the first row excitations. Furthermore, sulfur and silicon K-edge spectra are shown for 1-propanthiol and $Si(CH_3)_3Cl$, computed with the SRC-1 functional parameterized for the second row excitations. The computed spectra agree well with the experimental spectra, and it is not necessary to apply any shift to the excitation energies.

For butadiene, the calculation reproduces the essential features of the experimental spectrum well. Two peaks at 284.7 eV and 285.4 eV that correspond to C(1s) $\rightarrow$ π* excitations are predicted. The peak at low energy arises from excitation from the core orbitals on the end carbon atoms, while the peak at 285.4 eV arises from the 1s orbitals of the central carbon atoms. The broader peak at higher energy has contributions from a number of excitations. Peaks at 288.4 eV correspond to excitations to the higher energy π* orbital, while additional peaks arise from excitation to Rydberg 3p orbitals. The experimental spectrum of ethane has a sharp peak at 288.4 eV with a shoulder on the low energy side and a broad band at 291.4 eV, which lies above the ionization threshold. The calculations predict four excitations with non-zero intensity below 289 eV that correspond to excitations to 3s and 3p Rydberg states that lie broadly in agreement with the experimental spectrum. Above the ionization threshold the calculations show a number of significant bands, the most intense of which arises from excitation to a σ^*_{C-H} orbital.

The experimental spectrum for 1-propanethiol has a broad intense peak at 2472 eV, with a very broad band at higher energy above the ionization threshold. The calculations show two intense bands at 2472.8 eV and 2473.6 eV, in good agreement with the first band in the experiment. These excitations correspond to excitations from the 1s orbital of sulfur to virtual orbitals localized on the thiol group. These orbitals are described best as σ^*_{S-H} and σ^*_{C-S} consistent with earlier assignment.[52] Two distinct peaks are evident in the experimental spectrum of $Si(CH_3)_3Cl$. The first peak has been assigned to a Si(1s) $\rightarrow$ σ^*_{Si-Cl} excitation.[52] The calculations predict an intense band in good agreement with this. The calculations suggest that the second intense band has several contributions. Analysis of the orbitals is less definitive for this transition and suggests that the excitation corresponds to a mixture of excitation to σ^*_{C-Si} and carbon 3p Rydberg orbitals.

Plastocyanin is a copper-containing metalloprotein that is involved in electron transfer. The highest occupied molecular orbital of the active site is a singly occupied orbital that is a mixture of the $3d_{x^2-y^2}$ orbital of copper and the 3*p* orbitals of the sulfur ligand. Experiments have shown the pre-edge features in the copper and sulfur X-ray absorption spectra to lie at 8978 and 2469 eV.[3,53–55] Using a model of the active site

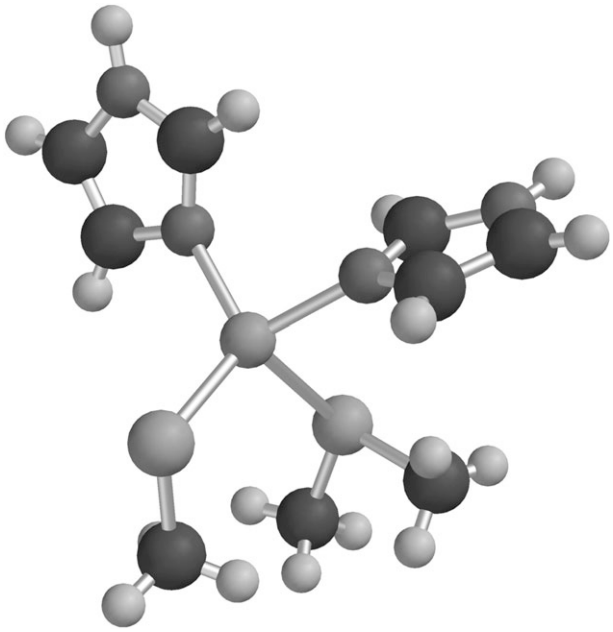

Fig. 5 Active site of plastocyanin.

(Fig. 5) and the SRC-1 functional optimized for the second row nuclei with the 6-31(2+,2+)G** basis set, Cu(1s) → 3d and S(1s) → 3d excitation energies are predicted to be 8977.8 eV and 2469.2 eV, once corrected for relativity. These values reproduce the experimental measurements and are much more accurate than the corresponding B3LYP values of 8863 eV and 2417 eV. It is quite surprising that an accurate value is predicted for the excitation from the copper 1s orbital since copper has a significantly higher nuclear charge than the nuclei used in the parameterization of the functional. This suggests that this functional can be applied to a wider range of systems comprising heavier nuclei than the second row elements, although it performs poorly for the first row core excitations, predicting excitation energies that are too high.

IV. Conclusions

Generalized gradient approximation and standard hybrid exchange–correlation functionals underestimate core excitations. This failure is associated with the approximate description of exchange. The application of long-range corrected functionals do not correct this underestimation of core excitation energies illustrating that the self-interaction at short and mid-range is important. Flexible new expressions for a range-corrected exchange–correlation functional with increased fractions of HF exchange in the short and long range regions were introduced. Optimization of these functionals to predict core excitation energies shows that increased HF exchange in the short range region is important. It has not been possible to find a single functional that corrects both core excitations for first and second row nuclei, and functionals for first and second row nuclei have been optimized separately. The resulting functionals reduce the error in the computed core excitation energies significantly and show what characteristics of range-corrected functionals are important for core excitations. This illustrates the importance of a correct description of the core region, which is not provided by many functionals. Further testing of the functionals to predict NEXAFS spectra for molecules not included in the fitting data shows that the spectra computed with the new functionals are in good agreement with experiment, and reproduce the essential features of the experimental spectra without the need to scale or shift the calculated spectra. Furthermore, the pre-edge features in the X-ray absorption spectra of plastocyanin for the copper and sulfur edges are predicted correctly, suggesting that the functional may be applied to heavier nuclei.

These functionals have been designed purely for the calculation of core excitation energies and the associated intensities, and have not been tested on the prediction of other molecular properties. Recent work has shown that long-range corrected functionals designed to give accurate valence excitation energies can lead to poorer results for ground state properties.[74] However, if short-range corrected functionals only affect the core orbitals and leave the valence orbitals unchanged, then it is more likely the performance of the functional for other properties can be maintained. This is consistent with very recent work involving short-range corrected functionals.[75] Furthermore, the functionals may improve results for other properties which are influenced by the core region. We are currently investigating this further.

References

1 J. Stöhr, *NEXAFS Spectroscopy, Springer Series in Surface Science*, Springer, Heidelberg, 1996.
2 J. G. Chen, *Surf. Sci. Rep.*, 1997, **30**, 1.
3 E. I. Solomon, R. K. Szilagyi, S. D. George and L. Basumallick, *Chem. Rev.*, 2004, **104**, 419.
4 C. J. Doonan, L. Zhang, C. G. Young, S. J. George, A. Deb, U. Bergmann, G. N. George and S. P. Cramer, *Inorg. Chem.*, 2005, **44**, 2579.
5 J. A. Sheehy, T. J. Gil, C. L. Winstead, R. E. Farren and P. W. Langhoff, *J. Chem. Phys.*, 1989, **91**, 1796.
6 H. Ågren, V. Carravetta, O. Vahtras and L. G. M. Pettersson, *Chem. Phys. Lett.*, 1994, **222**, 75.
7 L. Triguero, L. G. M. Pettersson and A. Ågren, *Phys. Rev. B: Condens. Matter Mater. Phys.*, 1998, **58**, 8097.
8 N. A. Besley, A. T. B. Gilbert and P. M. W. Gill, *J. Chem. Phys.*, 2009, **130**, 124308.
9 P. S. Bagus, *Phys. Rev.*, 1965, **139**, A619.
10 H. Hsu, E. R. Davidson and R. M. Pitzer, *J. Chem. Phys.*, 1976, **65**, 609.
11 A. Naves de Brito, N. Correla, S. Svensson and H. Ågren, *J. Chem. Phys.*, 1991, **95**, 2965.
12 A. T. B. Gilbert, N. A. Besley and P. M. W. Gill, *J. Phys. Chem. A*, 2008, **112**, 13164.
13 M. Stener, G. Fronzoni and M. de Simone, *Chem. Phys. Lett.*, 2003, **373**, 115.
14 N. A. Besley and A. Noble, *J. Phys. Chem. C*, 2007, **111**, 3333.
15 S. D. George, T. Petrenko and F. Neese, *Inorg. Chim. Acta*, 2008, **361**, 965.
16 U. Ekström and P. Norman, *Phys. Rev. A: At., Mol., Opt. Phys.*, 2006, **74**, 042722.
17 U. Ekström, P. Norman, V. Carravetta and H. Ågren, *Phys. Rev. Lett.*, 2006, **97**, 143001.
18 A. Nakata, Y. Imamura and H. Nakai, *J. Chem. Phys.*, 2006, **125**, 064109.
19 A. Nakata, Y. Imamura and H. Nakai, *J. Chem. Theory Comput.*, 2007, **3**, 1295.
20 G. Tu, Z. Rinkevicius, O. Vahtras, H. Ågren, U. Elkström, P. Norman and V. Carravetta, *Phys. Rev. A: At., Mol., Opt. Phys.*, 2007, **76**, 022506.

21 Y. Imamura and H. Nakai, *Int. J. Quantum Chem.*, 2007, **107**, 23.
22 J.-W. Song, M. A. Watson, A. Nakata and K. Hirao, *J. Chem. Phys.*, 2008, **129**, 184113.
23 Y. Imamura and H. Nakai, *Chem. Phys. Lett.*, 2006, **419**, 297.
24 F. A. Asmuruf and N. A. Besley, *Chem. Phys. Lett.*, 2008, **463**, 267.
25 A. Dreuw, J. Weisman and M. Head-Gordon, *J. Chem. Phys.*, 2003, **119**, 2943.
26 Y. Tawada, T. Tsuneda, S. Yanagisawa, T. Yanai and K. Hirao, *J. Chem. Phys.*, 2004, **120**, 8425.
27 T. Yanai, D. P. Tew and N. C. Handy, *Chem. Phys. Lett.*, 2004, **393**, 51.
28 M. J. G. Peach, A. J. Cohen and D. J. Tozer, *Phys. Chem. Chem. Phys.*, 2006, **8**, 4543.
29 O. A. Vydrov and G. E. Scuseria, *J. Chem. Phys.*, 2006, **125**, 234109.
30 J.-W. Song, T. Hirosawa, T. Tsuneda and K. Hirao, *J. Chem. Phys.*, 2007, **126**, 154105.
31 J.-W. Song, S. Tokura, T. Sato, M. A. Watson and K. Hirao, *J. Chem. Phys.*, 2007, **127**, 154109.
32 J.-D. Chai and M. Head-Gordon, *J. Chem. Phys.*, 2008, **128**, 084106.
33 J.-D. Chai and M. Head-Gordon, *Chem. Phys. Lett.*, 2008, **467**, 176.
34 M. A. Rohrdanz, K. M. Martins and J. M. Herbert, *J. Chem. Phys.*, 2009, **130**, 054112.
35 J. Heyd, G. E. Scuseria and M. Emzerhof, *J. Chem. Phys.*, 2003, **118**, 8207.
36 J. Heyd, J. E. Peralta, G. E. Scuseria and R. L. Martin, *J. Chem. Phys.*, 2005, **123**, 174101.
37 E. Batista, J. Heyd, R. G. Henning, B. P. Uberuaga, R. L. Martin, G. E. Scuseria and C. J. Umrigar, *Phys. Rev. B: Condens. Matter Mater. Phys.*, 2006, **74**, 121102.
38 P. J. Hay, R. L. Martin, J. Uddin and G. E. Scuseria, *J. Chem. Phys.*, 2006, **125**, 034712.
39 T. M. Henderson, A. F. Izmaylov, G. E. Scuseria and A. Savin, *J. Chem. Phys.*, 2007, **127**, 221103.
40 T. M. Henderson, A. F. Izmaylov, G. E. Scuseria and A. Savin, *J. Chem. Theory Comput.*, 2008, **4**, 1254.
41 S. Hirata and M. Head-Gordon, *Chem. Phys. Lett.*, 1999, **314**, 291.
42 A. Dreuw and M. Head-Gordon, *Chem. Rev.*, 2005, **105**, 4009.
43 N. A. Besley, *Chem. Phys. Lett.*, 2004, **390**, 124.
44 F. A. Asmuruf and N. A. Besley, *J. Chem. Phys.*, 2008, **129**, 064705.
45 A. D. Becke, *Phys. Rev. A: At., Mol., Opt. Phys.*, 1988, **38**, 3098.
46 C. Lee, W. Yang and R. G. Parr, *Phys. Rev. B: Condens. Matter Mater. Phys.*, 1988, **37**, 785.
47 S. H. Vosko, L. Wilk and M. Nusair, *Can. J. Phys.*, 1980, **58**, 1200.
48 M. Reiher and A. Wolf, *J. Chem. Phys.*, 2004, **121**, 2037.
49 H.-J. P Werner, P. J. Knowles, R. Lindh, F. R. Manby, M. Schütz, P. Celani, T. Korona, G. Rauhut, R. D. Amos, A. Bernhardsson, A. Berning, D. L. Cooper, M. J. O. Deegan, A. J. Dobbyn, F. Eckert, C. Hampel, G. Hetzer, A. W. Lloyd, S. J. McNicholas, W. Meyer, M. E. Mura, A. Nicklass, P. Palmieri, R. Pitzer, U. Schumann, H. Stoll, A. J. Stone, R. Tarroni and T. Thorsteinsson, *MOLPRO, version 2006.1, a package of ab initio programs*, 2006.
50 Y. Shao, L. F. Molnar, Y. Jung, J. Kussmann, C. Ochsenfeld, S. T. Brown, A. T. B. Gilbert, L. V. Slipchenko, S. V. Levchenko, D. P. O'Neill, R. A. DiStasio Jr, R. C. Lochan, T. Wang, G. J. O. Beran, N. A. Besley, J. M. Herbert, C. Y. Lin, T. V. Voorhis, S.-H. Chien, A. Sodt, R. P. Steele, V. A. Rassolov, P. E. Maslen, P. P. Korambath, R. D. Adamson, B. Austin, J. Baker, E. F. C. Byrd, H. Dachsel, R. J. Doerksen, A. Dreuw, B. D. Dunietz, A. D. Dutoi, T. R. Furlani, S. R. Gwaltney, A. Heyden, S. Hirata, C.-P. Hsu, G. Kedziora, R. Z. Khalliulin, P. Klunzinger, A. M. Lee, M. S. Lee, W. Liang, I. Lotan, N. Nair, B. Peters, E. I. Proynov, P. A. Pieniazek, Y. M. Rhee, J. Ritchie, E. Rosta, C. D. Sherrill, A. C. Simmonett, J. E. Subotnik, H. L. Woodcock III, W. Zhang, A. T. Bell, A. K. Chakraborty, D. M. Chipman, F. J. Keil, A. Warshel, W. J. Hehre, H. F. Schaefer III, J. Kong, A. I. Krylov, P. M. W. Gill and M. Head-Gordon, *Phys. Chem. Chem. Phys.*, 2006, **8**, 3172.
51 M. J. G. Peach, P. Benfield, T. Helgaker and D. J. Tozer, *J. Chem. Phys.*, 2008, **128**, 044118.
52 K. Yoshi, Y. Baba and T. A. Sasaki, *Phys. Status Solidi B*, 1998, **206**, 811.
53 S. E. Shadle, J. E. Penner-Hahn, H. J. Schugar, B. Hedman, K. O. Hodgson and E. I. Solomon, *J. Am. Chem. Soc.*, 1993, **115**, 767.
54 S. J. George, M. D. Lowery, E. I. Solomon and S. P. Cramer, *J. Am. Chem. Soc.*, 1993, **115**, 2968.
55 D. W. Randall, S. D. George, B. Hedman, K. O. Hodgson, K. Fujisawa and E. I. Solomon, *J. Am. Chem. Soc.*, 2000, **122**, 11620.
56 M. Tronc, G. C. King and F. H. Read, *J. Phys. B: At. Mol. Phys.*, 1979, **12**, 137.
57 M. Tronc, G. C. King and F. H. Read, *J. Phys. B: At. Mol. Phys.*, 1980, **13**, 999.
58 A. P. Hitchcock and C. E. Brion, *J. Phys. B: At. Mol. Phys.*, 1981, **14**, 4399.
59 C. T. Chen, Y. Ma and F. Sette, *Phys. Rev. A: At., Mol., Opt. Phys.*, 1989, **40**, 6737.
60 M. Domke, C. Xue, A. Puschmann, T. Mandel, E. Hudson, D. A. Shirley and G. Kaindl, *Chem. Phys. Lett.*, 1990, **173**, 122.
61 Y. Ma, C. T. Chen, G. Meigis, K. Randall and F. Sette, *Phys. Rev. A: At., Mol., Opt. Phys.*, 1991, **44**, 1848.
62 G. Remmers, M. Domke, A. Puschmann, T. Mandel, C. Xue, G. Kaindl, E. Hudson and D. A. Shirley, *Phys. Rev. A: At., Mol., Opt. Phys.*, 1992, **46**, 3935.
63 J. T. Francis, C. Enkvist, S. Lunell and A. P. Hitchcock, *Can. J. Phys.*, 1994, **72**, 879.
64 R. Püttner, I. Dominguez, T. J. Morgan, C. Cisneros, R. F. Fink, E. Rotenberg, T. Warwick, M. Domke, G. Kaindl and A. S. Schlachter, *Phys. Rev. A: At., Mol., Opt. Phys.*, 1999, **59**, 3415.
65 J. Adachi, N. Kosugi, E. Shigemasa and A. Yagishita, *Chem. Phys. Lett.*, 1999, **309**, 427.
66 R. B. Robin, *Chem. Phys. Lett.*, 1975, **31**, 140.
67 S. Bodeur and J. M. Esteva, *Chem. Phys.*, 1985, **100**, 415.
68 S. Bodeur, P. Millie and I. Nenner, *Phys. Rev. A: At., Mol., Opt. Phys.*, 1990, **41**, 252.
69 E. Gedat, R. Püttner, M. Domke and G. Kaindl, *J. Chem. Phys.*, 1998, **109**, 4471.
70 R. G. Cavell and A. Jürgensen, *J. Electron Spectrosc. Relat. Phenom.*, 1999, **101–103**, 125.
71 O. Nayandin, E. Kukk, A. A. Wills, B. Langer, J. D. Bozek, S. Canton-Rogan, M. Wiedenhoeft, D. Cubaynes and N. Berrah, *Phys. Rev. A: At., Mol., Opt. Phys.*, 2001, **63**, 062719.
72 A. P. Hitchcock and C. E. Brion, *J. Electron Spectrosc. Relat. Phenom.*, 1977, **10**, 317.
73 A. Naves de Brito, S. Svensson, N. Correia, M. P. Keane, H. Ågren, O. P. Sarinen, A. Kivimäki and S. Aksela, *J. Electron Spectrosc. Relat. Phenom.*, 1992, **59**, 293.
74 M. A. Rohrdanz and J. M. Herbert, *J. Chem. Phys.*, 2008, **129**, 034107.
75 T. M. Henderson, A. F. Izmaylov, G. Scalmani and G. E. Scuseria, *J. Chem. Phys.*, 2009, **131**, 044108.

